# Characterization of Ground and Low-Lying Excited States of $CoO_4$: A Combined Matrix Isolation and DFT Study

**Delphine Danset, Mohammad E. Alikhani,* and Laurent Manceron***

*LADIR/Laboratoire de Dynamique, Interactions et Réactivité/CNRS UMR 7075- Université Pierre et Marie Curie, case 49, 4 place Jussieu 75252 Paris, France*

*Received: June 19, 2004; In Final Form: August 26, 2004*

The nature of the reaction products between $CoO_2$ and molecular $O_2$, isolated in rare gas matrices, have been investigated using IR absorption spectroscopy. In this paper, we report on the vibrational spectrum of the $CoO_4$ molecule in its ground and first low-lying excited states. Isotopic substitutions using $^{16}O_2$ and $^{18}O_2$ precursors, as well as $^{16}O_2 + {}^{18}O_2$ and $^{16}O_2 + {}^{16}O^{18}O + {}^{18}O_2$ mixtures in either excess argon or neon, enable demonstration of $C_{2v}$ and $C_s$ structures for the respective states. $CoO_4$ is formed following molecular diffusion by complexation of ground-state $CoO_2$ by an $O_2$ molecule. The molecule is first formed in the excited state and then spontaneously relaxes to the ground state after remaining in the dark. The kinetics of relaxation can be fitted to a first-order exponential decay with an excited-state lifetime estimated around 23 ± 2 min in argon and 15 ± 2 min in neon, indicative of a slow, spin-forbidden process. Population of the excited state is induced by photons around 4250 ± 250 $cm^{-1}$. Experimental results are compared to density functional theory (DFT) calculations at the BPW91/6-311G(3df) level. Electronic and geometrical optimizations were carried out starting from the ground-state precursors (i.e., $^3\Sigma_g^-$ for $O_2$ and $^2\Sigma_g^+$ for $CoO_2$). Calculations predict a $^2A_2$ ($C_{2v}$) ground state and a $^4A'$ ($C_s$) first excited state 0.37 eV above, close to the 4250 ± 250 $cm^{-1}$ experimental excitation energy. The transition pathway is found to involve two supplementary states with crossed potential energy surfaces (PESs): a $^2B_1$ excited state, 0.48 eV above the ground state, reached first through an adiabatic transition with a photon around 4800 $cm^{-1}$, and a $^4B_1$ transition state into which the system relaxes before finally attaining the $^4A'$ ($C_s$) excited state. Harmonic frequencies and absolute intensities are also calculated and compared with the experimental data, indicating however that the DFT underestimates the internuclear distances for both configurations. Force and interaction constants were obtained with a semiempirical harmonic force-field potential calculation. They were then used in an empirical rule of plot linking force constants and internuclear distances in order to obtain an estimate of the Co−O bond lengths for each state and are compared to the DFT predictions.

## Introduction

The reactivity of molecular oxygen at the surface of cobalt single crystals, thin films, or cobalt oxide powders has given rise to many studies in the catalysis field.[1−3] These studies demonstrate that bulk cobalt surfaces react immediately to oxygen exposure to form $Co_3O_4$ crystals as a first step and then a more stable CoO crystal at saturation or upon heating the substrate to about 450 K. However, isolated Co atoms, in cobalt-substituted Schiff's base complexes, bind $O_2$ molecularly and have thus been thoroughly studied for their properties as oxygen carriers.[4−6] The geometrical and electronic structures of the complexed $O_2$ molecules on the cobalt center, as well as the exploration of reversible processes induced by temperature variations or chemical exposure, have been the center of these studies.

At the atomic level, the Co + $O_2$ system has been studied in both the gas and condensed phases. In the gas phase, the CoO diatomic species has been thoroughly studied,[7−9] and the $(CoO_2)^-$ anion isolated for photodetachment spectroscopy studies,[10] but larger neutral species, containing four or more atoms, remain to be fully characterized. Gas-phase studies also focused on the reactivity of isolated Co atoms toward molecular oxygen[11] regardless of the product nature, whereas condensed-phase studies in rare gas (RG) matrices[12,13] or zeolites[14] studied mostly the reaction products and their respective chemical and structural properties. Our knowledge of molecular cobalt oxides, aside from the diatomics and $CoO_2$ triatomics,[15] is in fact quite limited. Matrix isolation studies have offered the possibility of isolating otherwise unobservable species because of their short lifetime, but the Co + $O_2$ system has proven to be quite difficult. Chertihin et al.[13] studied the reaction of laser-ablated cobalt atoms with $O_2$ isolated in solid argon through FTIR spectroscopy and were among the first to characterize several cobalt oxides of higher stoichiometry, such as $CoO_4$. In their work, three isomers of $CoO_4$ were allegedly observed and each characterized by two fundamental vibrations. The first is an $(O_2)CoO_2$ isomer with two absorptions at 797.3 and 897.3 $cm^{-1}$, the second is an $OOCoO_2$ isomer with absorptions at 805.6 and 954.7 $cm^{-1}$, and finally, the third is ($(O_2)$CoOO), with absorptions at 1042.5 and 1365.3 $cm^{-1}$. Concentration and photophysical effects will rapidly show that, with one exception, all these bands cannot be correlated to species of $CoO_4$ stoechiometry.

Cobalt oxides have also been of interest at the theoretical level. Ab initio and DFT calculations have been carried out in an attempt to more completely understand the nature of the

* To whom correspondence should be addressed. E-mail: lm@ccr.jussieu.fr (L.M.), ea@spmol.jussieu.fr (M.E.A.).

10.1021/jp0473265 CCC: $30.25 
Published on Web 12/15/2004

reactivity and chemical bonding of these species as well as their electronic and structural properties.[16,17] Unfortunately, because of the closely placed valence orbital levels and near-degeneracy effects, this system has remained quite a challenge for theoretical treatment, and the predictive aspect of the calculations is not always satisfactory. For instance, Uzunova et al.[17] studied the $CoO_4$ molecule in its ground and excited states at the B1LYP/CCSD(T) levels. They predicted a $^6B_2$ ground state, with a diperoxide structure of $D_{2d}$ symmetry. They calculated $^2B_1$ and $^4A_2$ excited states, respectively 0.32 and 0.49 eV above the ground state, both with diperoxide ($D_{2d}$) structures. Calculations of the harmonic vibrational frequencies of the ground state (at the B1LYP level) place the $b_2$ (IR active) mode corresponding to the out-of-phase stretching mode of the O═O bonds, at 1153 $cm^{-1}$, and the in-phase stretch of the O═O bonds ($a_1$ symmetry, not IR active) at 1144 $cm^{-1}$. The other modes are calculated to be much lower at 483 (e), 477 ($b_2$), 365 ($a_1$), 321 (e), and 183 ($b_1$) $cm^{-1}$, among which only the e and $b_2$ modes are IR active with respective absolute intensities of 1, 0, and 4 km·$mol^{-1}$ compared to 155 for the $b_2$ mode at 1153 $cm^{-1}$. Calibration of their results on experimental data was difficult because of the few existing spectroscopic observations for this specific species. Nonetheless, the calculated frequencies did not match what had been proposed by Chertihin et al.[13]

In this paper, we present results on the $CoO_4$ molecule isolated in solid argon and neon, as well as observations of a low-lying excited state. A complete vibrational analysis of these two states is presented, and structural as well as electronic properties are discussed. The formation pathway of this molecule is also presented and discussed. The kinetics of relaxation is fitted to a first-order exponential decay supplying the lifetime of the excited state. DFT calculations have also been performed at the BPW91/6-311G(3df) level, supplying harmonic frequencies and electronic and geometrical structures, as well as the transition pathway from the ground to the excited state. Finally, a semiempirical harmonic force-field calculation (SHHF) is performed using the geometries obtained by the DFT calculations supplying a set of force and interaction constants for both states, reproducing as closely as possible the isotopic shifts. The force constants obtained for the Co−O bonds of each state will be used in the empirical correlation developed in ref 18, for CoO and its excited states, to propose some bond length estimates.

## Experimental Methods

Samples were formed in the same manner as described in the preceding article,[15] and details of the experimental setup can be found in refs 15 and 18. Samples were submitted for UV−vis broadband photolysis, using a HgXe arc with a converging lens focusing the light on the sample for 15 min. Irradiations were performed through a $CaF_2$ window mounted on the assembly. Total UV power was measured on the order of magnitude of 650 mW/$cm^2$.

After acquiring spectra in the mid-IR region from 500 to 5000 $cm^{-1}$, the sample was left in the dark for 1 to 8 h. Spectra taken after the relaxation were done using low-pass and band-pass IR filters mounted on a rotating wheel inside the spectrometer, at the exit of the interferometer, cutting off part of the light emitted by the source (SiC globar). Four different filters were used: $\nu < 1750$ $cm^{-1}$, $\nu < 1900$ $cm^{-1}$, $\nu \in [3500-3800]$ $cm^{-1}$ and $\nu < 4250$ $cm^{-1}$.

Further IR irradiations were done on the sample using a globar coupled to a large parabolic collection mirror to increase photon density. Broadband and filtered irradiations were performed, using combinations of low-pass and band-pass filters placed before the fluorine window, to isolate narrower effective energy ranges. Irradiation lasted for 30 to 60 min. The narrowest effective combination was a band-pass filter isolating $\nu \in [3700-4500]$ $cm^{-1}$. Total irradiation power in the absence of filters was measured at about 950 mW/$cm^2$, which is estimated to be about 60 times that of the spectrometer source. Irradiation power through the effective filter combination is measured to be 75 mW/$cm^2$.

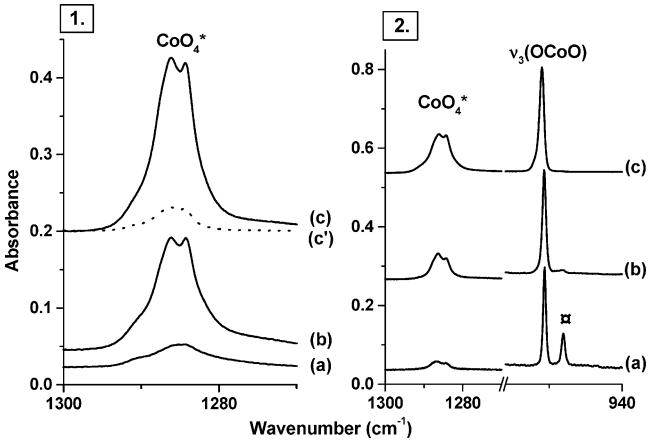


**Figure 1.** (1) IR spectra in the 1300−1270 $cm^{-1}$ region for thermally evaporated Co atoms codeposited with 2% $^{16}O_2$ in argon at 12 K; $\nu_1$ of $CoO_4$*: (a) deposition, (b) broadband UV photolysis, **(c)** annealing to 25 K, **(c′)** same as c, but after remaining in the dark 2 h, spectra taken using 1750 $cm^{-1}$ low-pass filter. (2) Comparison of the $\nu_1$ absorption of $CoO_4$* and $\nu_3$ of OCoO after deposition. ⌖ band due to a larger species: (a) Co + 0.5% $^{16}O_2$/Ar, (b) Co + 2% $^{16}O_2$/Ar, (c) Co + 8% $^{16}O_2$/Ar.

## Experimental Results

Samples were prepared by codeposition of effusive beams of Co atoms and $O_2$−RG mixtures onto a rhodium-plated copper mirror maintained at cryogenic temperatures. Both argon and neon matrices were used to estimate possible perturbations induced by the environment on the isolated species. In argon, the temperature was stabilized at 12 K during deposition and lowered to 3 K for spectral acquisition. Samples were deposited for 90 to 120 min, and concentrations varied from 0.5% to 16% $O_2$ in Ar, with a deposition rate of $5 \times 10^{-6}$ mol/min. Co/Ar molar ratios were typically on the order of $2 \times 10^{-3}$.

In neon, the temperature was maintained at 6.5 K during deposition and lowered to 3 K for spectral acquisition. Samples were deposited for 45 to 60 min, and concentrations varied from 200 to 2000 ppm $O_2$ in Ne, with a deposition rate of $2 \times 10^{-5}$ mol/min. Co/Ne molar rations were typically on the order of $5 \times 10^{-4}$. In neon, concentrations were lowered to compensate for easier diffusion in the matrix; nonetheless, the product yield in neon remains several times lower than that in argon. However, no qualitative change in the chemistry of the system is observed when changing the matrix, only slight frequency shifts and changes in the absorption profiles (i.e., absorption bands are usually narrower in neon, and band-splitting due to multiple-site effects is much more prevalent).

Directly after deposition, the band at 1286.2 $cm^{-1}$, attributed by Chertihin et al.[13] to an asymmetric peroxide form of $CoO_2$, is weakly observable. It grows considerably upon UV irradiation and yet again after annealing the sample (25 K in argon/11.5 K in neon) (Figure 1.1). When the sample is annealed directly after deposition, the species responsible for this absorption is not nearly formed in the same yield. Concentration effects show

**TABLE 1: Experimental Frequencies ($cm^{-1}$) and Relative Intensities (in parentheses) for the Excited-State $CoO_4$* Isolated in Solid Argon and Neon for All Isotopic Precursors**

| $CoO_4$* | | | | | | |
|---|---|---|---|---|---|---|
| $^{16}O_2$ | | | $^{18}O_2$ | | $^{16}O_2 + {}^{18}O_2$ | $^{18}O^{16}O$ |
| Ar | | Ne | Ar | | Ne | Ar | Ar |
| 1747.7 | (0.007) | 1765.8 | 1670.1 | (0.004) | 1688.3 | | 1709.2 |
| 1286.2 | (1) | 1285.0 | 1215.3 | (1) | 1213.5 | [a] | 1253.3/1250.2 |
| 953.1 | (0.147) | 961.8 | 916.8 | (0.166) | 925.3 | | 937.4 |
| 805.8 | (0.090) | 815.5 | 763.8 | (0.080) | 772.9 | | 782.4 |
| 382.6 | (0.013) | | 364.7 | (0.007) | | | |
| 374.1 | (0.002) | | 357.5 | (0.007) | | | |
| 198.7 | (0.025) | 204.3 | 191.0 | (0.021) | 196.2 | 194.0 | |
| 156.1 | (0.023) | 160.2 | 149.2 | (0.017) | 153.0 | 152.6 | |

[a] Not resolved or overlapped by other isotopic species.

that this species has indeed a linear dependence with respect to Co concentration but a quadratic dependence with respect to $O_2$ concentration. In Figure 1.2, three separate samples are presented that have been synthesized by keeping the Co concentration constant and changing the $O_2$ concentration from 0.5% to 2% and finally 8%. The band observed at 944.1 $cm^{-1}$ on Figure 1.2a, marked ⊙, belongs to a species containing more than two Co atoms. When the $Co/O_2$ ratio is lowered, this band disappears, as can be seen in on spectra b and c in Figure 1.2. Comparison of the integrated intensities ($I$'s) between the $\nu_3$ mode of OCoO at 945.5 $cm^{-1}$ and the 1286.2 $cm^{-1}$ band, when going from 0.5% to 2% and from 2% to 8%, shows that the $I(1286.2)/I(945.5)$ ratio is proportional to the $O_2$ concentration increase, indicating that the species responsible for this absorption contains an additional $O_2$ molecule and is therefore $CoO_4$.

Along with this absorption, several other bands at 953.1 and 805.8 $cm^{-1}$ in the mid-IR and 382.6, 374.1, 198.7, and 156.1 $cm^{-1}$ in the far-IR region are observed to follow an identical behavior following irradiation and annealing. They showed the same dependence to Co and $O_2$ concentrations and are attributed to the same species (Table 1).

Low-pass and band-pass filters mounted on a rotating wheel inside the spectrometer were used to keep part of the light emitted by the source from reaching the sample. Four different filters were used: $\nu < 1750$ $cm^{-1}$, $\nu < 1900$ $cm^{-1}$, $\nu \in [3500-3800]$ $cm^{-1}$, and $\nu < 4250$ $cm^{-1}$. Spectra taken using the 1750 and 1900 $cm^{-1}$ low-pass filters revealed a slow decrease of the 1286.2, 953.1, and 805.8 $cm^{-1}$ bands and a concomitant growth of another set of bands at 950.6, 898.2, and 842.8 $cm^{-1}$. After leaving the sample in the dark for 2 h, the 1286.2, 953.1, and 805.8 $cm^{-1}$ absorptions had almost completely disappeared (Figure 2), while the other three bands had grown considerably. When the 1750 $cm^{-1}$ low-pass filter was replaced by the low-pass 4250 $cm^{-1}$ filter, spectra showed a slow return of the 1286.2, 953.1, and 805.8 $cm^{-1}$ bands and a slight decrease of the other three. The filters were then removed completely from the spectrometer beam, and spectra were taken using the full range of the source. The 1286.2, 953.1, and 805.8 $cm^{-1}$ bands grew back completely, and the three bands at 950.6, 898.2, and 842.8 $cm^{-1}$ disappeared. Let it be noted that the photon flux supplied by the spectrometer source is estimated around 0.7 $mW/cm^2$ in the effective energy range and is thereby very low, but appears nonetheless sufficient to induce a complete switch from one set of absorption bands to the other during an unfiltered spectral acquisition, which can last up to 20 min. To follow adequately the decrease of the 1286.2, 953.1, and 805.8 $cm^{-1}$ absorption bands and the growth of the other set of bands, spectra of only a few scans (lasting less than a minute) using the 1750 $cm^{-1}$ low-pass filter were taken regularly every minute. The decreasing integrated intensity of the 1286.2 $cm^{-1}$ absorption as a function of the time is reported in Figure 3, along with the growing integrated intensity of the 950.6 $cm^{-1}$ band. The kinetics can be fitted to the same first-order exponential growth and decrease which indicates that both species are involved in the same slow process along an A ↔ B path. The half-life is calculated to be 23 ± 2 min in argon and 15 ± 2 min in neon. The time scale is on the order of magnitude of several minutes, which is very long for excited states.

In the far-IR region, samples were submitted to external IR irradiation to reproduce the excitation−relaxation process observed in the mid-IR region. A globar SiC, identical to the IR source of the spectrometer, was used, and irradiation was done through the $CaF_2$ window mounted on the assembly. Spectra taken before the irradiation, in the far-IR region, show

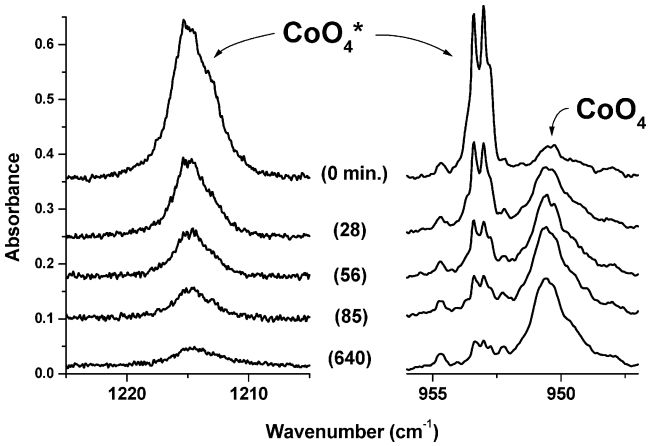


**Figure 2.** $CoO_4$* to ground-state $CoO_4$ relaxation kinetics in argon: IR spectra in the 1225−1205 and 955−940 $cm^{-1}$ regions taken using a 1750 $cm^{-1}$ low-pass filter after leaving sample in the dark for $t$ min.

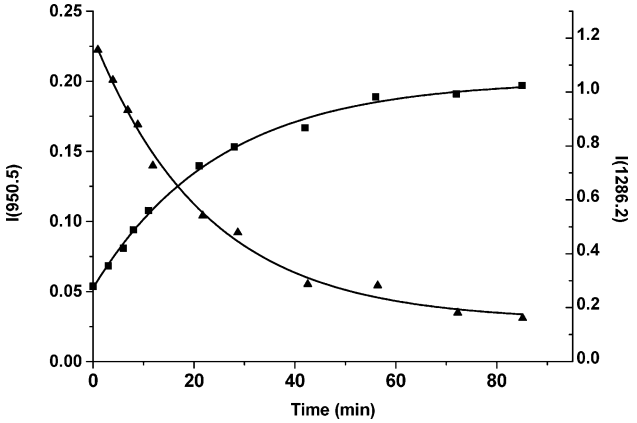


**Figure 3.** First-order exponential fit (growth and decay) for ■ Integrated intensity of $\nu_1$ of $CoO_4$, $I(950.6)$; ▲ Integrated intensity of $\nu_1$ of $CoO_4$*, $I(1286.2)$; as a function of the time obtained from bands presented Figure 2.

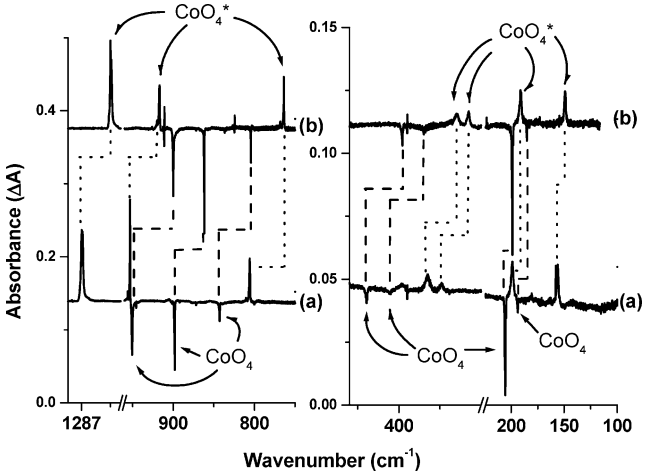


**Figure 4.** Difference of IR spectra in the mid- and far-IR regions in argon (spectra without low-pass filter minus spectra with low-pass filter after 2 h in the dark). Bands of $CoO_4$* are pointing upward, and bands of ground-state $CoO_4$ are pointing downward. (a) Co + $^{16}O_2$, (b) Co + $^{18}O_2$.

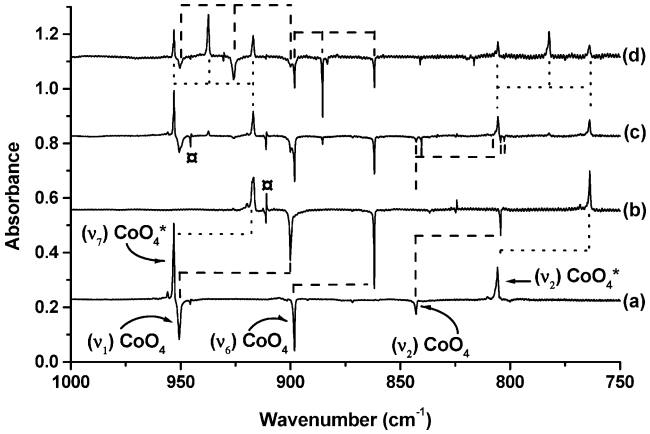


**Figure 5.** Difference of IR spectra in the 1000−750 $cm^{-1}$ region (spectra without low-pass filter minus spectra with low-pass filter after 2 h in the dark) for $CoO_4$ (pointing downward) and $CoO_4$* (pointing upward) fundamental absorptions with different isotopic mixtures. ⌖ bands due to OCoO isotopomer. (a) Co + $^{16}O_2$, (b) Co + $^{18}O_2$, (c) Co + [$^{16}O_2$ + $^{18}O_2$], (d) Co + [$^{16}O_2$ + $^{16}O^{18}O$ + $^{18}O_2$].

bands at 419.6, 405.7, 276.9, and 205.5 $cm^{-1}$ that have the same Co and $O_2$ dependency as $CoO_4$. Spectra taken directly after irradiation show growth of several new bands at 382.6, 374.0, 198.8, and 156.1 $cm^{-1}$ and disappearance of the four previous bands. After leaving the sample in the dark for 1 h, these bands vanished, and the previous bands at 419.6, 405.7, 276.9, and 205.5 $cm^{-1}$ grew back. This process was repeated several times, showing perfect reproducibility of the respective behaviors of both sets of bands (Figure 4).

When samples were annealed in the dark and spectra taken during the annealing process with the 1750 $cm^{-1}$ low-pass filter in the mid-IR region, the growth of the 1286.2, 953.1, and 805.8 $cm^{-1}$ bands was first observed. This shows that the $CoO_2$ + $O_2$ reaction proceeds without any barrier to the excited state of $CoO_4$. Frequencies and relative integrated intensities are reported in Tables 1 and 2. The 1286.2, 953.1, 805.8, 382.6, 374.0, 198.8, and 156.1 $cm^{-1}$ bands all correlate with the excited state: $CoO_4$*. The bands at 950.6, 898.2, 842.8, 419.6, 405.7, 276.9, 205.5, and 193.7 $cm^{-1}$ belong to the ground state: $CoO_4$.

Results obtained by isotopic substitutions will be described for each state separately. For the $CoO_4$ ground state, in samples containing $^{18}O_2$/Ar(Ne) mixtures, the 950.6 $cm^{-1}$ band is red-shifted by 50.9 $cm^{-1}$, while the 898.2 and 842.8 $cm^{-1}$ bands are shifted by 36.4 and 38.4 $cm^{-1}$, respectively (Figure 4). The bands of the far-IR region show shorter red shifts of 21.8 and 20.0 $cm^{-1}$ for the 419.6 and 405.7 bands and 14.4, 6.8, and 8.5 $cm^{-1}$ for the 276.9, 205.5, and 193.7 $cm^{-1}$ absorptions, respectively (Figure 4). In samples containing an equal 50%−50% mixture of $^{16}O_2$ and $^{18}O_2$, isotopic multiplets are sometimes more clearly observable in neon samples than in argon because of the fact that the absorption bands are narrower in neon. Therefore, the observation of small couplings between the vibrational modes is facilitated in neon, whereas they sometimes remain unresolved in argon, because the bands overlap. The band at 950.6 $cm^{-1}$ presents a quartet structure composed of the two bands observed in the $^{16}O_2$/Ar and $^{18}O_2$/Ar samples and of two supplementary bands at 949.6 and 901.2 $cm^{-1}$. The 898.2 $cm^{-1}$ absorption reveals a triplet structure with a supplementary band at 862.1 $cm^{-1}$, very close to the absorption of the $Co^{18}O_2$ isotopomer. The profile of the 898.2 $cm^{-1}$ band is not broadened in these samples, but its relative intensity is greater than what would be expected, implying that two bands are overlapped at this frequency and that the multiplet has in fact a quartet structure. Finally, the 842.8 $cm^{-1}$ absorption presents supplementary bands at 840.3, 806.1, and 802.8 $cm^{-1}$ (Figure 5). In the far-IR region, the absorptions at 419.6, 276.9, and 205.5 $cm^{-1}$ show resolved quartet structures. The band at 405.7 $cm^{-1}$ is too weak to be observed in samples containing more than one isotopic species. In samples containing ($^{16}O_2$ + $^{18}O^{16}O$ + $^{18}O_2$)/Ar mixtures, all modes in the mid-IR range present a middle component. The 885.4 $cm^{-1}$ band is slightly blue-shifted and the 816.5 $cm^{-1}$ slightly red-shifted, with respect to the exact middle of the isotopic interval delimited by the absorptions of $Co^{16}O_4$ and $Co^{18}O_4$ (Figure 5). In the far-IR region, only the

**TABLE 2: Experimental Frequencies ($cm^{-1}$) and Relative Intensities (in parentheses) for Ground-State $CoO_4$ Isolated in Solid Argon and Neon for All Isotopic Precursors**

| $CoO_4$ | | | | | | |
|---|---|---|---|---|---|---|
| $^{16}O_2$ | | | $^{18}O_2$ | | $^{16}O_2 + {}^{18}O_2$ | $^{18}O^{16}O$ |
| Ar | | Ne | Ar | | Ne | Ar | Ar |
| 1727.5 | (0.023) | 1742.4 | 1651.0 | (0.025) | 1667.0 | | |
| 950.6 | (1) | 957.9 | 900.1 | (1) | 907.5 | 949.6/901.2 | 925.9 |
| 898.2 | (0.752) | 905.7 | 861.8 | (0.558) | 869.1 | −/862.1 | 885.4 |
| 842.8 | (0.235) | 847.6 | 804.3 | (0.209) | 812.9 | 840.3/806.1/802.8 | 816.5 |
| 419.6 | (0.039) | | 397.9 | (0.026) | 404.2 | 417.57/401.70 | |
| 405.7 | (0.007) | | 384.7 | (0.006) | | | |
| 276.9 | (0.012) | | 262.5 | (0.021) | 265.0 | 275.2/264.1 | 269.6 |
| 205.5 | (0.162) | 208.4 | 198.8 | (0.135) | 201.3 | 203.9/200.4 | 199.6/201.0/201.8/202.8/204.7 |
| 193.7 | (0.013) | 196.7 | 185.2 | (0.006) | 188.3 | 190.2/189.0 | |

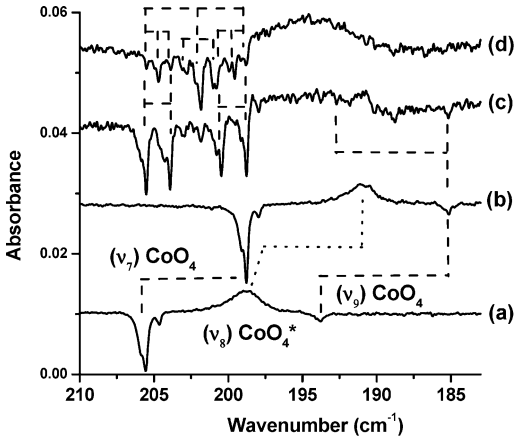


**Figure 6.** Difference of IR spectra in the far-IR region (spectra without low-pass filter minus spectra with low-pass filter after 2 h in the dark) for $CoO_4$ (pointing down) and $CoO_4$* (pointing up) fundamental absorptions with different isotopic mixtures. (a) Co + $^{16}O_2$, (b) Co + $^{18}O_2$, (c) Co + [$^{16}O_2$ + $^{18}O_2$], (d) Co + [$^{16}O_2$ +$^{16}O^{18}O$ + $^{18}O_2$].

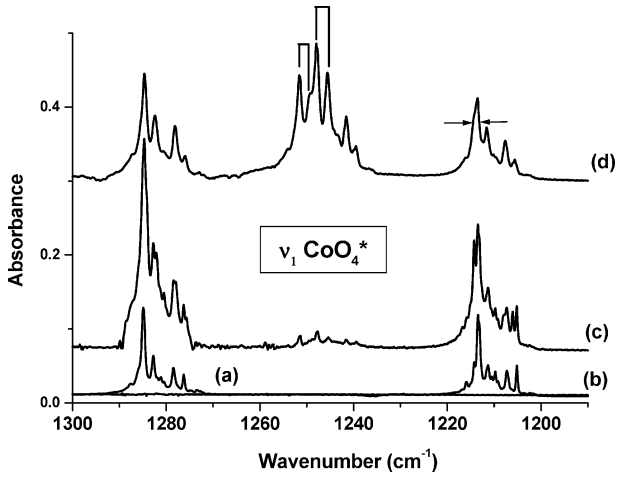


**Figure 7.** IR spectra in the $\nu_1$ region of $CoO_4$* in neon with different isotopic mixtures. (a) Co + $^{16}O_2$, (b) Co + $^{18}O_2$, (c) Co + [$^{16}O_2$ + $^{18}O_2$], (d) Co + [$^{16}O_2$ +$^{16}O^{18}O$ + $^{18}O_2$].

205.5 $cm^{-1}$ mode reveals all nine components of a resolved triplet of triplets (Figure 6) characteristic for molecules with two pairs of equivalent O atoms. The other absorptions in this region are too weak to be observed as isotopic multiplets.

For the $CoO_4$* excited state, when replacing $^{16}O_2$ by $^{18}O_2$, the 1286.2 $cm^{-1}$ absorption is red-shifted by 70.9 $cm^{-1}$, while the 953.1 and 805.8 $cm^{-1}$ bands are red-shifted by 36.3 and 42 $cm^{-1}$, respectively. The weaker bands in the far-IR region at 382.6, 374.0, 198.8, and 156.1 $cm^{-1}$ are red-shifted by 17.9, 16.5, 7.7, and 6.9 $cm^{-1}$, respectively. In samples containing an equal mixture of $^{16}O_2$ and $^{18}O_2$, multiplet structures are more clearly resolved in neon. The 1286.2 $cm^{-1}$ band shows a quartet structure (see Figure 6 of the preceding article[15]), only resolved in neon at an 0.1 $cm^{-1}$ resolution. The 953.1 $cm^{-1}$ band shows a doublet structure, but the absorption profiles are broadened in samples containing ($^{16}O_2$ +$^{18}O_2$)/RG mixtures compared to those of samples containing only one isotopic species ($^{16}O_2$/RG or $^{18}O_2$/RG). This indicates that additional bands are present in the isotopic multiplet, but remain unresolved, even in neon. For the 805.8 $cm^{-1}$ absorption, a resolved quartet structure is observed with ($^{16}O_2$ +$^{18}O_2$) precursors showing new bands at 805.5 and 765.4 $cm^{-1}$ (Figure 5). The bands in the far-IR region at 382.6, 374.0, 198.8, and 156.1 $cm^{-1}$, once again, have broadened absorption profiles leaving the isotopic multiplets unresolved. Finally, in samples containing $^{16}O_2$, $^{18}O^{16}O$, and $^{18}O_2$ precursors, the multiplets around 1286.2 and 1215.3 $cm^{-1}$ present broadened signals near the absorptions of the $Co^{16}O_4$ and $Co^{18}O_4$ molecules, thus indicating the presence of several unresolved additional isotopic components (see arrows on Figure 7d). Only the central component near 1250 $cm^{-1}$ shows a clear 3.1 $cm^{-1}$ splitting due to the $^{16}O^{18}OCoO_2$ and $^{18}O^{16}OCoO_2$ isotopomer groups (Figure 7). For the two other main absorptions of this system at 953.1 and 805.8 $cm^{-1}$, a middle component is observed in the presence of $^{16}O_2$, $^{18}O^{16}O$, and $^{18}O_2$ precursors. Absorptions in the far-IR region are too weak to show resolved isotopic multiplets in the presence of these precursors.

Chertihin et al.[13] had assigned several different absorption bands to $CoO_4$ isomers, and it is important that these assignments be revised before we go on with our discussion concerning the $CoO_4$ species. The bands at 1042 and 1365 $cm^{-1}$, assigned to $OOCo(O_2)$, cannot belong to the same species; indeed, when the sample is submitted to HgXe broadband photolysis, the 1042 $cm^{-1}$ absorption disappears, while the 1365 $cm^{-1}$ absorption grows along with a band at 1331 $cm^{-1}$, tentatively assigned to $CoO_3$ by Chertihin et al.[13] Concentration effects show that the 1331 and 1365 $cm^{-1}$ bands are absent in very diluted samples (0.5% $O_2$/Ar) but are prevalent in concentrated samples (8−16% $O_2$/Ar), after annealing. They have the same dependence on Co and $O_2$ concentrations and present identical behaviors: growing considerably after photolysis and annealing above 25 K. The species responsible for these absorptions shows a higher-order dependence toward $O_2$ than $CoO_4$ and will be designated as $CoO_y$, with $y > 4$ (species Y of the previous publication). The concentration effects also show that two supplementary bands at 797.3 and 897.3 $cm^{-1}$ (Figure 8a) show the same dependence on both $O_2$ and Co as $CoO_y$. Furthermore, these two bands show the same behavior to photolysis and annealing as the 1331 and 1365 $cm^{-1}$ bands and are, therefore, assigned to $CoO_y$ as well. Experiments done in isotopically substituted samples, such as ($^{16}O_2$ + $^{18}O_2$) mixtures, show that the 1331 and 1365 $cm^{-1}$ bands present complex multiplet structures, and in samples containing ($^{16}O_2$ + $^{18}O^{16}O$ + $^{18}O_2$) mixtures, the isotopic multiplets are not triplets but contain many overlapping supplementary bands (Figure 8b). Therefore, with the exception of the 805.6 $cm^{-1}$ band assigned to $OOCoO_2$, all other bands belong, in fact, to larger species. The study of these larger species is not our aim in this paper, and they will not be discussed further.

## Theoretical Results

Calculations have been carried out using the same DFT method as that used in the preceding article (BPW91/6-311G-(3df)).[15] Indeed, for $CoO_2$, the CCSD(T) method was used as well to obtain the most promising results. Unfortunately, such calculations were not feasible for $CoO_4$ at our level. Nonetheless, the DFT results obtained in the preceding article are in acceptable agreement with the experimental data for $CoO_2$ and will be used as a starting point. The dissociation energies were calculated with respect to the ground-state fragments ($^3\Sigma_g^-$ for $O_2$ and $^2\Sigma_g^+$ for $CoO_2$) correlating with a quartet surface.

All structures have been considered and calculations optimized for $C_1$, $C_s$, $C_{2v}$, $D_{2d}$ and $T_d$ symmetries, taking into account all spin multiplicities (doublet, quartet, and sextet) each time. Only two structures were found to be competitive at low energy, corresponding to $^2A_2$ ($C_{2v}$) and $^4A'$ ($C_s$) states. The sextet state ($^6B_2$ ($D_{2d}$)) obtained by Uzunova et al.[17] was found to be at higher energies: 0.80 eV above the ground state. Energies

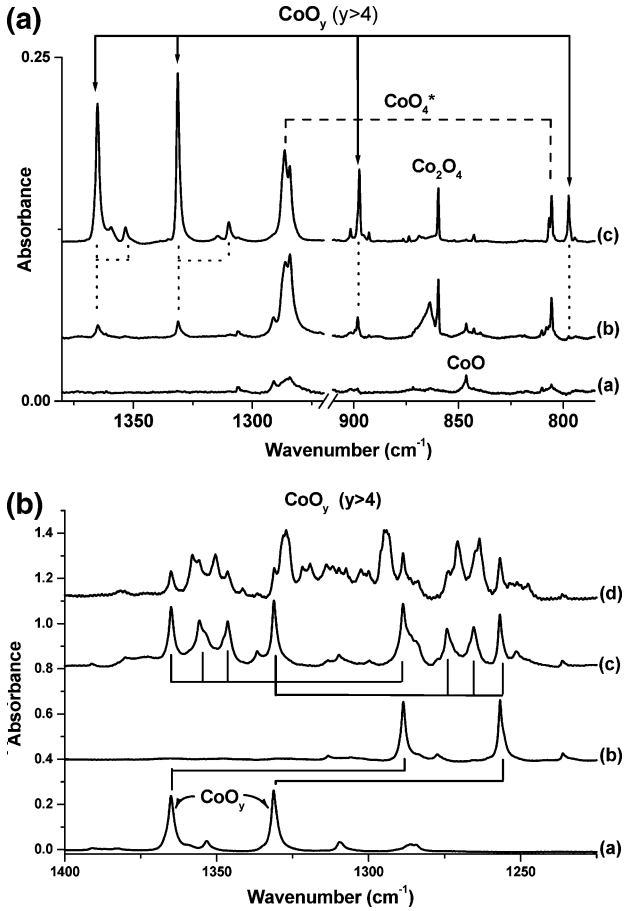


**Figure 8.** (part a) IR spectra in the 1380−750 cm$^{-1}$ region for thermally evaporated Co atoms codeposited with 2% $^{16}O_2$/Ar. Fundamental absorptions of $CoO_y$, $y > 4$, and $CoO_4$* in argon: (a) deposition, (b) UV broadband photolysis, (c) annealing to 30 K. Spectra has been multiplied by 0.28 to normalize on the band at 1286.2 cm$^{-1}$ of $CoO_4$*. (part b) IR spectra in the 1400−1225 cm$^{-1}$ region. Fundamental absorptions of $CoO_y$, $y > 4$, in argon with different isotopic mixtures: (a) Co + $^{16}O_2$, (b) Co + $^{18}O_2$, (c) Co + [$^{16}O_2$ + $^{18}O_2$], (d) Co + [$^{16}O_2$ + $^{16}O^{18}O$ + $^{18}O_2$].

for sextet mutiplicities for $C_{2v}$ and $C_s$ symmetries were found at 0.60 and 0.76 eV, respectively, showing that the sextet states are all well above the doublet and quartet states. We verified that spin contamination was in every case lower than 5% with respect to the expected values ($\langle S^2 \rangle = 0.75$, 3.75, or 8.75 for the doublet ($s = {}^1/_2$), quartet ($s = {}^3/_2$) or sextet ($s = {}^5/_2$) states). Figure 9 presents the optimized geometries for the doublet and quartet states and binding energies (BEs) with respect to those of the ground-state fragments. The real minima in the doublet and quartet manifolds are the $^2A_2$ and $^4A'$ structures which have been fully optimized. The $^4B_1$ structure is not a real minimum but a transition state obtained with a $C_{2v}$ symmetry constraint, which relaxes to the $^4A'$ state once the constraint is removed.

Figure 10 presents the potential energy profiles calculated for each state in the transition pathway along the O−OCoO bisector angle coordinate. The $^4B_1$ state is a transition state and is accessed through an adiabatic transition with an imposed $C_{2v}$ symmetry constraint ($\alpha_1 = \alpha_2$). The $\Delta S = 0$ electronic selection rule being respected, this transition is fully allowed and should have a very high transition moment and short lifetime. The $^2B_1$ excited state and the $^4B_1$ potential energy profiles are calculated to cross below the vertical transition. The system in this picture, therefore, relaxes easily to the $^4B_1$ state without reaching the bottom of the $^2B_1$ potential energy surface (PES). It then finally relaxes to the $^4A'$ state which is a true local minima of the quartet

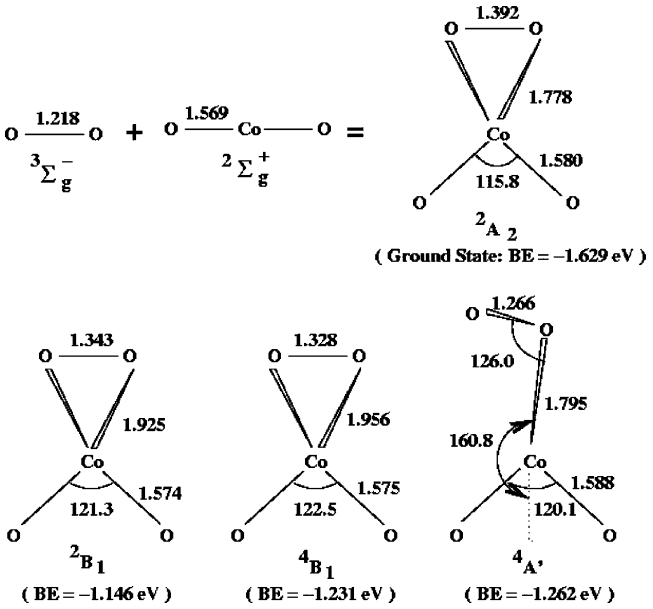


**Figure 9.** Optimized geometries at the BPW91/6-311G(3df) level for ground-state reactant and low-lying states of the $O_2 + CoO_2 \rightarrow CoO_4$ system. Distances are in angstroms (Å) and angles in degrees (°).

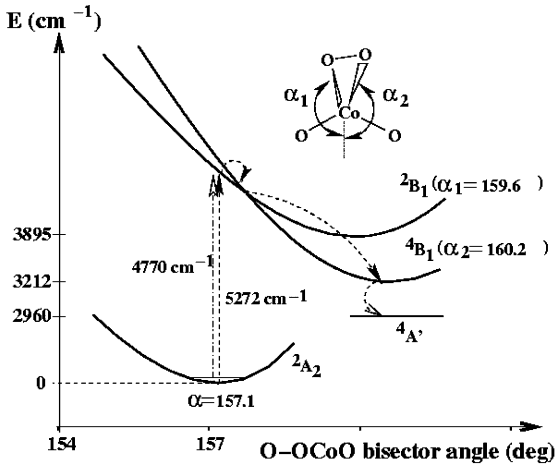


**Figure 10.** Potential energy profiles of the $^2A_2$, $^2B_1$, and $^4B_1$ states along the angle between each O atom (of $O_2$) and the bisector of OCoO subunits (labeled as $\alpha_1$ and $\alpha_2$). For each value of $\alpha_1 = \alpha_2$, all of the remaining geometrical variables have been reoptimized.

manifold. The PES of the $^4A'$ state is not represented in Figure 10, because then, $\alpha_1 \neq \alpha_2$ and the O− OCoO bisector angle is no longer a pertinent coordinate. All four states are represented in Figure 11, placed at their respective energies.

Harmonic frequencies and absolute intensities have been calculated for the $^2A_2$ and $^4A'$ states for two isotopomers, $Co^{16}O_2$ and $Co^{18}O_2$, and are reported in Tables 3 and 4, along with the experimental frequencies and relative intensities for easier comparison.

## Discussion

A vibrational analysis, based on experimental results, will be done in order to discuss structures for both states of $CoO_4$. Next, the photophysical properties of this system, as well as a possible formation pathway, will be presented.

Experimental results and conclusions will then be compared with DFT and semiempirical harmonic force field potential (SHFF) calculations. Evolution of the bond force constants, geometries, and the transition pathway between states obtained by the DFT calculations will be discussed.

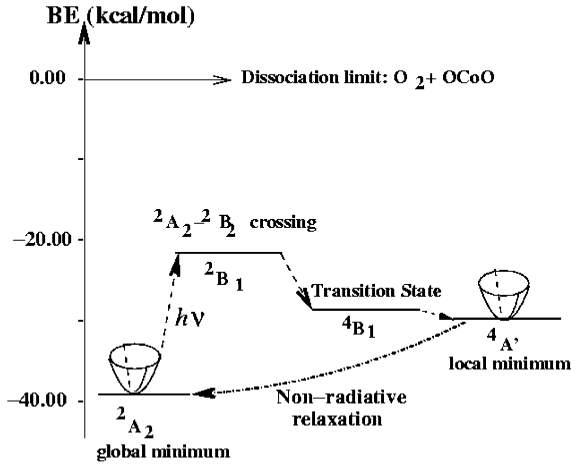


**Figure 11.** Representation of the different stages of the excitation−relaxation process of $CoO_4$. All states involved in the process are placed at their respective energies.

**A. Vibrational Analysis and Structural Implications.** The large differences observed in the frequencies of the lowest-lying states of $CoO_4$ indicate that a significant geometry change occurs when going from the ground to the excited state.

*$CoO_4$ Ground State.* For the ground state (GS), eight fundamental absorptions and one combination were observed. The isotopic quartets observed in samples containing $^{16}O_2 + {}^{18}O_2$ mixtures show that the O atoms in the molecular GS are two-by-two equivalent.

The large-frequency shift observed for the 950.6 $cm^{-1}$ fundamental when using $^{18}O_2$ precursors is typical of an O═O stretch of an $O_2$ group bonded in a superoxide form. The 419.6 and 405.7 $cm^{-1}$ absorptions are typically in the energy range of the elongations of a superoxide form, as observed in the case of $NiO_2$.[20] The observed isotopic shifts of −21.7 and −21 $cm^{-1}$, respectively, for these modes, when going from $Co^{16}O_2$ to $Co^{18}O_2$, as well as the large difference in the integrated intensities, clearly indicate that the 419.6 $cm^{-1}$ band is the asymmetric stretch and the 405.7 $cm^{-1}$ band is the symmetric stretch. The energy and isotopic patterns observed for the 898.2 and 842.8 $cm^{-1}$ bands are typical of Co—O stretching modes of a bent dioxo group. Respective isotopic shifts and integrated intensities show that the 842.8 $cm^{-1}$ band is the symmetric stretching mode and the 898.2 $cm^{-1}$ band is the asymmetric stretching mode of the OCoO-dioxo part of the molecule. A combination of these two modes is observed at 1727.5 $cm^{-1}$, supplying the crossed anharmonicity $X_{62} = -13.5$ $cm^{-1}$. It is interesting to note that this combination is very close to the $\nu_1 + \nu_3$ combination of isolated OCoO molecules at 1717.4 $cm^{-1}$,[13] and the crossed anharmonicity is also quite close to the $X_{13} = -11.7$ $cm^{-1}$ anharmonicity of OCoO.

The absorptions of the far-IR region are typical of bending modes. All these observations lead to a $C_{2v}$ structure, with a dioxo-superoxide form. Furthermore, even if the $^{18}O^{16}O$ counterpart of the asymmetric CoO stretching mode at 885.4 $cm^{-1}$ is blue-shifted with respect to the average of the $Co^{16}O_4$ and $Co^{18}O_4$ isotopic interval, it only indicates coupling between the CoO coordinates of the dioxo group. The fact that the profile of the 885.4 $cm^{-1}$ absorption is identical to that of the pure isotopic components implies that the symmetry lowering does not induce supplementary couplings between the dioxo and the superoxo groups with $^{18}O^{16}O$ substitutions, suggesting that the molecule is likely nonplanar and that the dioxo and superoxo moieties are in perpendicular planes.

A $C_{2v}$ structure leads to the decomposition of normal vibrational modes into irreducible representations spanning $\Gamma_{vib} = 4a_1 + a_2 + 2b_1 + 2b_2$. Aside from one movement of $a_2$ symmetry, which is not IR active and corresponds to a torsional vibration, all vibrational fundamentals are observed.

*$CoO_4$* Excited State.* For the excited state, seven fundamental absorptions and one combination are observed. The most intense

**TABLE 3: Comparison of Experimental (in solid argon) and DFT Calculated Frequencies ($cm^{-1}$) and Intensities for the $^2A_2$ State of $CoO_4$[a]**

| | frequencies for $Co^{16}O_4$ | | | | | frequencies for $Co^{18}O_4$ | | | | |
|---|---|---|---|---|---|---|---|---|---|---|
| | exptl | | calcd (DFT) | | | exptl | | calcd (DFT) | | |
| $\nu_1$ ($A_1$) | 950.6 | (1) | 1004.0 | [112] | (1) | 900.1 | (1) | 952.4 | [103] | (1) |
| $\nu_6$ ($B_1$) | 898.2 | (0.752) | 970.0 | [84] | (0.76) | 861.8 | (0.558) | 929.7 | [78] | (0.768) |
| $\nu_2$ ($A_1$) | 842.8 | (0.235) | 952.4 | [3] | (0.11) | 804.3 | (0.209) | 903.7 | [0.3] | (0.057) |
| $\nu_3$ ($A_1$) | 419.6 | (0.039) | 579.1 | [1] | (0.01) | 397.9 | (0.026) | 554.0 | [1] | (0.016) |
| $\nu_8$ ($B_2$) | 405.7 | (0.007) | 466.7 | [7] | (0.05) | 384.7 | (0.006) | 442.5 | [7] | (0.057) |
| $\nu_4$ ($A_1$) | 276.9 | (0.012) | 335.1 | [4] | (0.01) | 262.5 | (0.021) | 317.2 | [4] | (0.024) |
| $\nu_5$ ($A_2$) | | | 252.4 | [0] | (0) | | | 237.7 | [0] | (0) |
| $\nu_7$ ($B_1$) | 205.5 | (0.162) | 230.3 | [4] | (0.07) | 198.8 | (0.135) | 220.2 | [4] | (0.066) |
| $\nu_9$ ($B_2$) | 193.7 | (0.013) | 237.3 | [14] | (0.01) | 185.2 | (0.006) | 229.2 | [13] | (0.016) |

[a] Absolute IR intensities are in brackets [km/mol], and relative intensities are in parentheses.

**TABLE 4: Comparison of Experimental (in solid argon) and DFT Calculated Frequencies ($cm^{-1}$) and Intensities for the $^4A'$ State of $CoO_4$[a]**

| | frequencies for $Co^{16}O_4$* | | | | | frequencies for $Co^{18}O_4$* | | | | |
|---|---|---|---|---|---|---|---|---|---|---|
| | exptl | | calcd (DFT) | | | exptl | | calcd (DFT) | | |
| $\nu_1$ (A′) | 1286.2 | (1) | 1277.6 | [163] | (1) | 1215.3 | (1) | 1204.4 | [144] | (1) |
| $\nu_7$ (A″) | 953.1 | (0.147) | 971.0 | [67] | (0.406) | 916.8 | (0.166) | 931.5 | [62] | (0.425) |
| $\nu_2$ (A′) | 805.8 | (0.090) | 920.9 | [22] | (0.112) | 763.8 | (0.080) | 875.1 | [21] | (0.121) |
| $\nu_3$ (A′) | 382.6 | (0.013) | 513.9 | [8] | (0.029) | 364.7 | (0.007) | 490.1 | [7] | (0.027) |
| $\nu_4$ (A′) | 374.1 | (0.002) | 330.0 | [4] | (0.005) | 357.5 | (0.007) | 317.5 | [4] | (0.005) |
| $\nu_5$ (A′) | | | 284.6 | [5] | (0.020) | | | 270.7 | [4] | (0.016) |
| $\nu_8$ (A″) | 198.7 | (0.025) | 218.5 | [2] | (0.005) | 191.0 | (0.021) | 207.8 | [2] | (0.005) |
| $\nu_6$ (A′) | 156.1 | (0.023) | 150.2 | [16] | (0.064) | 149.2 | (0.017) | 143.1 | [15] | (0.072) |

[a] Absolute IR intensities are in brackets [km/mol], and relative intensities are in parenthesis.

**TABLE 5: Comparison of Experimental and Calculated Frequencies ($cm^{-1}$) for Ground-State $CoO_4$ in Solid Argon[a]**

| | $(^{16}O_2)Co^{16}O_2$ | | $(^{18}O_2)Co^{18}O_2$ | | $(^{16}O_2)Co^{18}O_2$ | | $(^{18}O_2)Co^{16}O_2$ | | $(^{16}O^{18}O)Co^{16}O^{18}O$ | |
|---|---|---|---|---|---|---|---|---|---|---|
| | obsd | calcd | obsd | calcd | obsd | calcd | obsd | calcd | obsd | calcd |
| $\nu_1$ ($A_1$) | 950.6 | 951.4 | 900.1 | 899.4 | 949.5 | 951.1 | 901.2 | 900.8 | 925.9 | 926.0 |
| $\nu_6$ ($B_1$) | 898.2 | 898.4 | 861.9 | 862.1 | *b* | 862.1 | 898.2 | 898.4 | 885.4 | 885.5 |
| $\nu_2$ ($A_1$) | 842.9 | 842.6 | 804.4 | 803.2 | 806.5/802.8[c] | 805.8 | 840.4 | 839.3 | 816.6 | 817.7 |
| $\nu_3$ ($A_1$) | 419.6 | 418.9 | 397.9 | 400.7 | 417.6 | 414.6 | 401.7 | 405.1 | 407.7 | 405.1 |
| $\nu_8$ ($B_2$) | 405.7 | 404.9 | 384.7 | 384.2 | *b* | 404.9 | *b* | 384.2 | 397.0 | 392.2 |
| $\nu_4$ ($A_1$) | 276.9 | 277.2 | 262.5 | 262.2 | 264.1 | 264.6 | 275.2 | 274.6 | 269.9 | 269.9 |
| $\nu_5$ ($A_2$) | | 272.8 | | 257.2 | | 269.6 | | 260.5 | | 265.3 |
| $\nu_7$ ($B_1$) | 205.5 | 205.3 | 198.8 | 198.2 | 200.5 | 200.2 | 203.9 | 203.4 | 201.9 | 201.7 |
| $\nu_9$ ($B_2$) | 193.8 | 193.7 | 185.2 | 185.0 | 189.0 | 188.7 | 190.2 | 190.1 | 188.9 | 189.1 |

[a] Semiempirical force-field calculations with $F_{OO} = 3.58$, $F_{Co=O} = 5.45$, $F_{Co-O} = 1.56$, $F_{CoO,\,CoO} = 0.15$, $F_{CoO,OO} = 0.405$, $F_{Co=O,OO} = 0.2$, $F_{Co=O,\,CoO} = -0.15$ mdyne/Å, $F_{\alpha} = 0.62$, $F_{\theta} = 0.625$, $F_{\alpha\alpha adj} = -0.42$, $F_{\alpha\alpha opp} = -0.05$ mdyne/Å $rad^2$. [b] Not resolved or overlapped by other isotopic species. [c] Presumed Fermi resonance doublet.

absorption is the 1286.2 $cm^{-1}$ band; the energy range is typical of that of an unruptured O═O bond stretching mode. The important isotopic shift observed for this mode (−70.9 $cm^{-1}$) when changing the $^{16}O_2$ precursor to $^{18}O_2$ is a clear indication that this absorption corresponds to a mode involving mainly an $O_2$ stretch. Additionally, the frequency of this mode is closer to that of a free oxygen molecule (∼1550 $cm^{-1}$) than in the GS, indicating that the O═O bond is less perturbed in this state. Furthermore, the Co—($O_2$) vibration occurs at a lower frequency, 382.6 $cm^{-1}$, indicating that the bond is quite weak. The quartet structure observed in samples containing an equal 50%−50% mixture of $^{16}O_2$ and $^{18}O_2$ precursors shows very short shifts between the $Co^{16}O_4$ and ($^{16}O_2$)Co($^{18}O_2$) absorption bands, thus indicating that the coupling between the O═O and Co—O coordinates is weak, and substitution of the other two oxygens of the molecule has a low impact on the frequency of the O═O stretch. Additionally, the isotopic multiplet observed in samples containing $^{16}O_2$, $^{16}O^{18}O$, and $^{18}O_2$ precursors indicates that the oxygens involved in this mode are nonequivalent.

The 953.1 and 805.8 $cm^{-1}$ bands are typical of Co—O stretching modes of a bent dioxo group. The smaller (−36.3 and −42.0 $cm^{-1}$) isotopic shifts observed when going from $^{16}O_2$ to $^{18}O_2$ precursors for these two modes are indications that these two oxygens are no longer linked. The triplet structures of the 953.1 and 805.8 $cm^{-1}$ bands in samples containing $^{16}O_2$, $^{18}O^{16}O$, and $^{18}O_2$ precursors imply that these two oxygens are equivalent. The relative intensities of these two absorption bands, respectively, 0.147 and 0.090, indicate that the 805.8 $cm^{-1}$ band, being the weakest, corresponds to the symmetric stretch of the oxygens and the 953.1 $cm^{-1}$ band, almost twice as intense as the previous, corresponds to the asymmetric stretch. The absorption observed at 1747.7 $cm^{-1}$ corresponds to the $\nu_7 + \nu_2$ combination and supplies the $X_{27} = -11.2$ $cm^{-1}$ crossed anharmonicity. Finally, with two equivalent oxygens fixed on the cobalt atom and two nonequivalent ones, a $C_s$ or $C_1$ symmetry is the only possibility for this state of the molecule.

**B. Structural Evolution and Comparison with DFT Calculations.** The 950.6 $cm^{-1}$ $\nu_1$ mode of the ground state corresponding to the O═O stretch is blue-shifted to 1286.2 $cm^{-1}$ ($\nu_1$ mode of the excited state) indicating that the O═O bond is strengthened in the excited state and therefore shortened. The isotopic multiplet of the 1286.2 $cm^{-1}$ band clearly shows that the oxyens are no longer two-by-two equivalent. Only the two O atoms of the dioxo part of the molecule remain equivalent, while the other two become nonequivalent, indicating that one of the Co—O bonds of the cycle has been ruptured. The remaining Co—O bond is very weakened and elongated compared to the original Co—O bonds of the cycle. The low-frequency modes at 419.6 and 405.7 $cm^{-1}$ of the ground state are red-shifted to 382.6 and 374.1 $cm^{-1}$, respectively, once again showing that the bond is weakened.

The asymmetric and symmetric stretches of the dioxo part of both molecules are also informative. Indeed, the 898.2 $cm^{-1}$ band is blue-shifted to 953.1 $cm^{-1}$, and the 842.9 $cm^{-1}$ band is red-shifted to 805.8 $cm^{-1}$, bringing the frequencies in the excited state closer to those of the isolated OCoO molecule, which is linear.[15] It appears that an opening of the OCoO angle occurs in the excited state which is coherent with a smaller perturbation induced by the other oxygens of the molecule, since the cycle has been broken and sterical hindrance is lessened. Note that the integrated intensities are quite different as well (Tables 1 and 2), supporting yet again the angle change toward linearity in the dioxo part of the molecule.

The DFT calculated geometrical parameters (angles and distances) of each state evolve according to the experimental data (Figure 9), yet the harmonic frequencies are not reproduced very well, implying, for instance, that the Co—O interatomic distances are largely underestimated. Indeed, for the GS, the $\nu_1$ frequency is calculated at 1003.9 $cm^{-1}$ instead of 950.6 $cm^{-1}$, which indicates that the O═O bond is longer than the 1.392 Å calculated. The $\nu_3$ and $\nu_8$ bands are calculated at 579.1 and 466.7 $cm^{-1}$ instead of 419.6 and 405.7 $cm^{-1}$, which shows that the Co—O bonds of the cycle are also quite underestimated by the calculations. The frequencies calculated for the dioxo part of the molecule are also too high, which means that the bond lengths are once again underestimated.

For the excited state, the same type of discrepancy appears. The $\nu_1$ frequency is calculated at 1277.6 $cm^{-1}$, which overestimates slightly the O═O bond length (1.266 Å). As for the $\nu_2$ vibration, it is calculated at 920.8 $cm^{-1}$ instead of 805.8 $cm^{-1}$, which is an error of 15%, suggesting that the calculated bond length is once again underestimated.

To check the consistency of the proposed geometry and vibrational assignments, as well as help compare the evolution of Co—O and O═O bond strengths in the $O_2 + CoO_2$ complexation or in the two different electronic states, a semiempirical harmonic force field calculation was developed, on the basis of the best reproduction of both frequencies and isotopic effects and the DFT geometry. The results are presented in Tables 5 and 6 and call for a few comments.

For the ground state, as discussed before, the O═O and Co—O coordinates are coupled in the $\nu_1$ and $\nu_2$ modes, a correct reproduction of the isotopic effects, such as the small shifts on $\nu_1$ when going from ($^{16}O_2$)$Co^{16}O_2$ to ($^{16}O_2$)$Co^{18}O_2$ or on $\nu_2$ going from ($^{16}O_2$)$Co^{16}O_2$ to ($^{18}O_2$)$Co^{16}O_2$, imposes severe constraints on the $F_{CoO,OO}$ interaction force constants which are determined within 0.05 N/cm. The model predicts, however, a 2.5 $cm^{-1}$ blue shift on $\nu_1$ in ($^{16}O_2$)$Co^{18}O_2$ relative to ($^{18}O_2$)$Co^{18}O_2$, when

**TABLE 6: Comparison of Experimental and Calculated Frequencies ($cm^{-1}$) for $CoO_4$ in the $^4A'$ State, Values Observed Solid Neon[a]**

| | $(^{16}O_2)Co^{16}O_2$ | | $(^{18}O_2)Co^{18}O_2$ | | $(^{16}O_2)Co^{18}O_2$ | | $(^{18}O_2)Co^{16}O_2$ | | $(^{16}O^{18}O)Co^{16}O^{18}O$ $(^{18}O^{16}O)Co^{16}O^{18}O$ | |
|---|---|---|---|---|---|---|---|---|---|---|
| | obsd | calcd | obsd | calcd | obsd | calcd | obsd | calcd | obsd | calcd |
| $\nu_1$ (A′) | 1286.2 | 1287.9 | 1215.3 | 1214.3 | 1285.5 | 1287.5 | 1214.4 | 1214.8 | 1253.3 | 1254.0 |
| | | | | | | | | | 1250.2 | 1249.4 |
| $\nu_7$ (A″) | 953.1 | 953.2 | 916.8 | 914.9 | *b* | 914.9 | *b* | 953.2 | 937.4 | 936.6 |
| | | | | | | | | | *b* | 936.6 |
| $\nu_2$ (A′) | 805.8 | 805.9 | 763.8 | 765.4 | 764.8 | 765.8 | 805.5 | 805.4 | 782.4 | 783.2 |
| | | | | | | | | | *b* | 783.1 |
| $\nu_3$ (A′) | 382.6 | 382.5 | 364.7 | 365.7 | *b* | 377.6 | *b* | 380.2 | *b* | 374.2 |
| | | | | | | | | | | 374.1 |
| $\nu_4$ (A′) | 374.1 | 374.6 | 357.5 | 355.6 | *b* | 364.4 | *b* | 356.3 | *b* | 369.1 |
| | | | | | | | | | | 361.4 |
| $\nu_5$ (A′) | | 251.5 | | 239.8 | | 249.2 | | 242.0 | | 245.6 |
| | | | | | | | | | | 245.1 |
| $\nu_8$ (A″) | 198.7 | 198.3 | 191.0 | 187.3 | *b* | 197.4 | *b* | 188.2 | *b* | 195.3 |
| | | | | | | | | | | 190.4 |
| $\nu_6$ (A′) | 156.1 | 156.5 | 149.2 | 150.4 | *b* | 151.9 | *b* | 155.1 | *b* | 152.8 |
| | | | | | | | | | | 154.2 |

[a] Semiempirical force-field calculations with $F_{OO} = 7.45$, $F_{Co=O} = 5.77$, $F_{Co-O} = 0.89$, $F_{CoO,\ CoO} = -0.28$, $F_{CoO,OO} = -0.25$, $F_{Co=O,OO} = 0.4$, $F_{Co=O,CoO} = 0.15$ mdyne/Å. $F_\alpha = 1.04$, $F_\theta = 0.72$, $F_{\alpha\alpha} = 0.97$, $F_{\alpha\theta} = 0.66$, $F_{torsion} = 0.05$ mdyne Å rad$^2$. [a] Not resolved or overlapped by other isotopic species.

only a band at 802.8 $cm^{-1}$ is clearly observed. We think that the occurrence of an anharmonic resonance, specific to this isotopic species, is responsible for this discrepancy. The first overtone of the band observed at 401.7 $cm^{-1}$ for this molecule would provide an almost perfect energy match, and the second, unobserved component of the Fermi dyad would come at higher frequency and be masked by the strong absorption at 805.8 $cm^{-1}$ for the normal isotopes (Figure 4). The reproduction of the observed isotopic shifts is otherwise satisfactory and within the small systematic deviations due to anharmonicity, except for the $\nu_3$ and $\nu_7$ bands, for which the errors on some isotopic shifts reach 15%. This usually signals a problem with the assumed geometry, such as a slightly too obtuse OCoO bond angle for the superoxide group. The overestimation of both the $A_1$ and $B_2$ Co($O_2$) stretching modes in the DFT results is in line with this conclusion, and it is likely that the true molecular geometry implies a longer Co—($O_2$) distance than what is implied here. By varying the potential constants around their optimal values, it is possible to estimate the O═O, Co═O, and Co—O force constants to 3.55 ± 0.1, 5.45 ± 0.1, and 1.55 ± 0.05 mdyne $Å^{-1}$, respectively.

To facilitate quantitative comparisons between cobalt dioxide, its oxygen-coordinated forms, or the different electronic states of the latter, we have also performed an SHFF calculation fitting harmonic potential constants to most accurately reproduce the frequencies and isotopic shifts on $CoO_4$* (Table 6). The experimental data are not as complete as for the ground state, in particular in the low frequency region, for which one IR-active fundamental is missing, and isotopic data in the mixtures are not clearly resolved, thus assignments follow the ordering predicted in the DFT calculation, which may be the cause of some discrepancies between the predicted and observed isotopic shifts. This model is thus only indicative in the low-frequency vibration region and can only be trusted for the stretching vibrations and motions above 300 $cm^{-1}$. The optimal values for the O═O, Co═O, and Co—O force constants amount to 7.45 ± 0.2, 5.77 ± 0.1, and 0.89 ± 0.1 mdyne $Å^{-1}$, respectively. Thus, the O═O bond force constant has an intermediate value between that in $O_2$ (11.35) and ionic superoxides (5.5, typically). Also, compared to the low-spin state, the Co═O bond is longer, within uncertainty equal to that found in $CoO_2$, and the Co—(O═O) bond force constant is almost half as large, a sign of a much looser interaction.

**TABLE 7: Force Constants (mdyne/Å) and Estimated Bond Lengths (Å) for the Co—O Bonds of the $^2A_2$ (GS) and $^4A'$ States of $CoO_4$**

| | force constant (SHHF) | $r_e$ (empirical estimate)[a] | $r_e$ (BPW91/ 6-311G(3df)) |
|---|---|---|---|
| $CoO_4$ ($^2A_2$) | $F_{Co=O} = 5.45$ | 1.628 | 1.580 |
| | $F_{Co-O} = 1.56$ | 1.834 | 1.778 |
| $CoO_4$* ($^4A'$) | $F_{Co=O} = 5.77$ | 1.618 | 1.588 |
| | $F_{Co-O} = 0.89$ | 1.927 | 1.795 |

[a] Error is estimated to be ±0.01Å.

Having obtained the main force constants for each state, we can propose an estimation of each bond length using a Herschbach—Laurie type empirical correlation optimized for the CoO diatomics. The bond length estimates are reported Table 7 along with those calculated by the DFT for easier comparison. For the $^2A_2$ state, $r_e = 1.628 \pm 0.010$ Å is obtained for the Co═O bonds of the dioxo Co—O bonds, and $r_e = 1.834 \pm 0.010$ Å is obtained for the Co—O bonds of the coordinated $O_2$.

For the $^4A'$ state, the Co═O bonds of the dioxo part of the molecules are estimated at $r_e = 1.618 \pm 0.01$ Å, which is consistent with what has been previously presented (i.e., those Co═O bonds are shortened when going from the ground to the excited state), possibly because of a reduction of the perturbation induced by the O═O bond and less steric hindrance. The Co—(O═O) bond, on the other hand, is very weakened in this state, and the estimated bond length is $r_e = 1.927 \pm 0.010$ Å, which is practically 0.15 Å longer than what was found by the DFT.

This rule, linking force constants and bond lengths, is quite accurate when optimized and used for a specific type of bond. The values presented here are only an estimate, but they give a good approximation of the bond lengths for these cobalt oxide molecules.

**C. Formation Pathway and Photophysical Properties.** The formation pathway of this molecule can be followed through the experimental observations. Indeed, to form this molecule, samples need to first be submitted to UV—vis broadband photolysis and then annealed to 25 K. The broadband photolysis

produces large quantities of OCoO, which decreases significantly upon annealing. Let it be noted that no species other than OCoO decreases with annealing the sample. In samples where the triatomic species is barely formed, $CoO_4$ is barely formed as well. Both of these indications tend to prove that the triatomic species fixes an oxygen molecule to form $CoO_4$. Also, the excited state is formed first, followed by relaxation to the ground state. Because it has been shown that the OCoO triatomic species has a $^2\Sigma_g^+$ ground state[21] and that $O_2$ has a $^3\Sigma$ ground state, reactants interact first on the quartet PES. Thus, it seems more likely that the excited state belongs to the quartet manifold. Additionally, the experimental data presented here show that the $D_{2d}$ geometry proposed by Uzunova et al. does not correspond to what is experimentally observed.

The photophysical properties of this molecule were also of interest, and several experimental observations lead to conclusions that will be confronted with DFT calculations.

An efficient energy range for the electronic transition has been isolated, within the $\nu = 4250 \pm 250$ cm$^{-1}$ interval. It is important to emphasize that this energy range is not the energy that separates ground and metastable states of $CoO_4$ but only the energy range of the photon that induces population of the excited state. Further observations tending to prove this affirmation are discussed hereafter. As it was observed, the light from the spectrometer source is sufficient to induce total transformation of the ground state into the excited state, when not filtered above 3800 cm$^{-1}$. Because of the very low photon density of the source, this would imply that the transition is a spin-allowed process. On the other hand, the relaxation of $CoO_4$* back to the ground state is very slow, indicating that this transition has a very low probability. Therefore, the ground state and the observed $CoO_4$* metastable state cannot have the same multiplicity. This implies that at least one supplementary state is involved in the excitation process and that this state has the same multiplicity as the ground state, making the transition completely allowed and with a very short lifetime. It is this intermediate state that is reached about $4250 \pm 250$ cm$^{-1}$ (0.52 eV) above the ground state. Additionally, this short-lived state must relax rapidly toward a state of the same multiplicity as the metastable state $CoO_4$*, and because this relaxation is not observed, it implies that the PESs of these two states should cross. Otherwise, two slow relaxation processes would be observed: one between the two intermediate states and another between metastable and ground states. Therefore, it seems that at least two supplementary states of different multiplicities are present in the activation process in order to fit the experimental observations.

The scheme proposed from the DFT calculations is consistent with these observations. The ground state of $CoO_4$ is calculated to be $^2A_2$ with a $C_{2v}$ structure, and the first excited state is $^4A'$ with a $C_s$ structure. The transition pathway involves two supplementary states of different spin multiplicities, as it was suggested through the analysis of the experimental data. The calculated energy of the adiabatic transition is 4770 cm$^{-1}$ (0.59 eV), which is in the vicinity of what was experimentally observed. Excitation from ground to the $^2B_1$ state is spin-allowed, and the $^2B_1-^4A'$ relaxation will be made efficient via the $^4B_1$ transition state, which has a geometry close to that of the $^2B_1$ state. The $^4A'$ state (0.36 eV above the ground state) represents a bottleneck in the relaxation process, because it could not relax without both a spin-forbidden process and a large geometry change (Figure 11). This is completely consistent with the long lifetime observed in rare gas matrices for the low-lying excited state of $C_s$ symmetry (23 to 15 min half-life, depending on the matrix nature). We did not attempt to estimate the energy barrier to overcome in the relaxation process nor its exact nature. It could possibly give rise to IR phosphorescence and remains to be investigated. It is interesting to note that Calatayud et al. [22] studied the $VO_4$ molecule at the B3LYP/6-31G* level and found very similar results to what was found here for $CoO_4$, as the species involve the same number of unpaired d-electrons. Indeed, their calculations start from the reaction of $VO_2$ ($^2A_1$) with $O_2$ ($^3\Sigma$) to form $CoO_4$. The ground state is calculated to be a $^2B_2$ of $C_{2v}$ symmetry, with oxygens two-by-two equivalent and the dioxo and superoxo moieties in perpendicular planes. The first excited state is found to be a $^4A$ ($C_1$), 2.6 eV above the ground state. Therefore, aside from the larger energy difference between the two states found for $VO_4$, the electronic structures and geometries resemble greatly what could be observed and calculated for $CoO_4$.

**Acknowledgment.** We wish to thank Danielle Carrère for her careful assistance in the experiments. This work was supported by C.N.R.S. Grant UMR 7075. One of us (M.E.A.) is grateful of allocation of computer time (IDRIS, CNRS, Grant 041730).

## References and Notes

(1) Klingerberg, B.; Grellner, F.; Borgmann, D.; Wedler, G. *Surf. Sci.* **1993**, *296*, 374.
(2) Jiménez, V. M.; Fernandez, A.; Espinos, J. P.; Gonzalez-Elipe, A. R. *J. Electron Spectrosc. Relat. Phenom.* **1995**, *71*, 61.
(3) Valeri, S.; Borghi, A.; Gazzadi, G. C.; di Bona, A. *Surf. Sci.* **1999**, *423*, 346.
(4) Basolo, F.; Hoffman, B. M.; Ibers, J. A. *Acc. Chem. Res.* **1975**, *8*, 384.
(5) Henson, N. J.; Hay, P. J.; Redondo, A. *Inorg. Chem.* **1999**, *38*, 1618.
(6) Hutson, N. D.; Yang, R. T. *Ind. Eng. Chem. Res.* **2000**, *39*, 2252.
(7) Clouthier, D. J.; Huang, G.; Merer, A. J.; Friedman-Hill, E. J. *J. Chem. Phys.* **1993**, *99*, 6336.
(8) Ram, R. S.; Jarman, C. N.; Bernath, P. F. *J. Mol. Spectrosc.* **1993**, *160*, 574.
(9) Barnes, M.; Clouthier, D. J.; Hajigeorgiou, P. G.; Huang, G.; Kingston, C. T.; Merer, A. J.; Metha, G. F.; Peers, J. R. D.; Rixon, S. J. *J. Mol. Spectrosc.* **1997**, *186*, 374.
(10) Wang, L. S. ref 36 in ref 13.
(11) Matsui, R.; Senba, K.; Honma, K. *J. Phys. Chem. A* **1997**, *101*, 179.
(12) Green, D. W.; Reedy, G. T.; Kay, J. G. *J. Mol. Spectrosc.* **1979**, *78*, 257.
(13) Chertihin, G. V.; Citra, A.; Andrews, L.; Bauschlicher, C. W., Jr. *J. Phys. Chem. A* **1997**, *101*, 8793.
(14) El-Malki, El-M.; Werst, D.; Doan, P. E.; Sachtler, W. M. H, *J. Phys. Chem. B* **2000**, *104*, 5924.
(15) Danset, D.; Alikhani, M. E.; Manceron, L. *J. Phys. Chem. A* **2005**, *109*, 97.
(16) Gutsev, G. L.; Rao, B. K.; Jenna, P. *J. Phys. Chem. A* **2000**, *104*, 5374.
(17) Uzunova, E. L.; Nikolov, G. St.; Mikosh, H. *J. Phys. Chem. A* **2002**, *106*, 4104.
(18) Danset, D.; Manceron L. *J. Phys. Chem. A* **2003**, *107*, 11324.
(19) Hunter, B.; Klinkhachorn, P.; Overton, E. B. *Rev. Sci. Instrum.* **1988**, *59*, 983.
(20) Danset, D.; Manceron, L.; Andrews L. *J. Phys. Chem. A* **2001**, *105*, 7205.
(21) Van Zee, R. J.; Hamrick, Y. M.; Li, S.; Weltner, W., Jr. *J. Phys. Chem.* **1992**, *96*, 7247.
(22) Calatayud, M.; Silvi, B.; Andrés, J.; Beltran, A. *Chem. Phys. Lett.* **2001**, *333*, 493.